Do CTs Like DC? Performance of Current Transformers With Geomagnetically Induced Currents

Bogdan Kasztenny, Normann Fischer, Douglas Taylor, Tejasvi Prakash, and Jeevan Jalli
Schweitzer Engineering Laboratories, Inc.

For the complete history of this paper, refer to the next page.

Presented at the
69th Annual Conference for Protective Relay Engineers
College Station, Texas
April 4–7, 2016

Originally presented at the
42nd Annual Western Protective Relay Conference, October 2015

Do CTs Like DC? Performance of Current Transformers With Geomagnetically Induced Currents

Bogdan Kasztenny, Normann Fischer, Douglas Taylor, Tejasvi Prakash, and Jeevan Jalli

Schweitzer Engineering Laboratories, Inc.

Abstract—**This paper analyzes the performance of current transformers (CTs) under the presence of geomagnetically induced currents (GICs). Our intent is to qualify the impact of GICs on CT performance in the context of protection security and dependability. The paper proposes a simple method to analyze the GIC problem and applies it to explain and quantify the impact of GICs on CTs. The paper uses carefully selected simulation tools, as well as laboratory tests on a physical CT to derive and support our key findings. We summarize our conclusions as follows: GIC impact is negligible in steady states during load conditions or faults but is significant in the first few milliseconds of a fault. As such, the GIC impact is very similar to the impact of the CT remanent flux on the performance of CTs during fault conditions. This impact is significant but short-lived. The component of CT saturation caused by high remanent flux or a preexisting GIC disappears very quickly.**

I. Introduction

Geomagnetically induced currents (GICs) are unipolar currents caused by Earth's magnetic storms that flow in transmission lines and circulate through system grounding points, typically through wye-connected transformer windings and autotransformers. To the system, GICs appear as a quasi direct current (dc) superimposed onto the nominal system frequency currents. GICs remain a concern for the electric power industry. New technical papers are written, and the industry comes together in newly formed working groups to look at the problem. The integrity of large, expensive, and difficult-to-replace assets (primarily power transformers and synchronous generators) is the primary concern in the GIC discussion. GICs, at least hypothetically, can be a wide-area phenomenon, and as such, they can potentially impact a multitude of transformers or generators, hence the concern of governments, regulators, and industry organizations.

The GIC problem is defined for power transformers as potential thermal damage caused by elevated excitation currents and stray flux closing outside of the transformer magnetic core. Further, the increased excitation current drawn by the transformers is harmonic-rich, which can cause problems for adjacent generators. In this case, the concern is the extra rotor heating caused by certain harmonic currents in the stator that establish a magnetic field rotating in the opposite direction to the rotor.

This paper focuses on the performance of current transformers (CTs) with GICs. In steady states, constant currents (such as GICs) are not transformed across the magnetic circuit of a CT but they offset the magnetic flux and increase CT errors. Therefore, we are concerned with protection security and dependability for faults and switching events that happen when the GICs are present in the primary currents.

CT saturation due to fault currents is well known. We understand the impact of CT burden, CT ratio, saturation voltage (C class), fault current level, system X/R ratio, or even remanent flux on the performance of protection CTs. We know how to specify a CT to avoid saturation and how to calculate time to saturation for cases when saturation cannot be avoided [1] [2].

Protective relays incorporate a number of mechanisms to manage CT saturation, ranging from a percentage restraint in differential relays to sophisticated external fault detectors that trigger on external faults before CTs saturate and potentially jeopardize protection security [2]. We know how to specify CTs to ensure protection dependability.

The presence of GICs is yet another, albeit less understood, factor that may impact the performance of protection CTs. Our goal is to characterize that impact in both qualitative and quantitative manners so that we can combine our findings into a complete set of rating calculations for a CT (together with the burden, X/R ratio, saturation voltage, and so on).

Section II reviews briefly the GIC phenomenon and explains the GIC levels we can expect in practice. This discussion is of great importance because the GIC level has a dramatic effect on the CT performance. Fortunately, the expected GIC levels are very small compared with CT ratings in transmission applications.

Section III presents and explains a simplified CT model that allows us to understand and characterize the impact of GIC, as well as the impact of all traditional factors, such as the X/R ratio of the system, CT burden, or saturation voltage. We introduce and use a novel signal model of the CT rather than the circuit model because the former allows better comprehension of the relevant phenomena.

Section IV analyzes CT performance with very low-frequency currents. First, we start with a single low-frequency current because we understand the impact of frequency on CT performance (we know how to derate a CT for lower frequencies). Next, we assume that the primary current signal contains a rated frequency current that represents the load or fault current and a very low-frequency current that represents

the GIC phenomenon. We use both computer simulations and laboratory tests to verify our surprising findings; while the low-frequency current is not reproduced well at all, the rated frequency current is reproduced with only minor errors.

Section V continues the analysis but assumes a strict dc current rather than a low-frequency current to represent the GIC. We conclude that the standing dc component has a minor impact on the CT performance when considering the rated frequency current.

Section VI looks specifically at CT performance during faults with preexisting GICs. Our observations are that the GIC impact in the steady state is relatively minor. In this respect, our findings are consistent with the fundamental 1981 work by Kappenman, Albertson, and Mohan [3]. However, we also find that the transient impact of the GIC is significant and similar to that of remanent flux. Section VI explains and illustrates this phenomenon in depth.

Section VII describes practical CT derating rules for GICs by providing numerical formulas for specifying CTs to avoid performance errors with preexisting GICs.

Finally, in Section VIII, we put our findings into perspective and explain the GICs' effect on protective relays. The key observation, congruent with everyday observations, is that GICs have no real impact on protection systems.

II. GIC PHENOMENON

The solar cycle describes the periodic nature of the sun's activity. The cycle is roughly 11 years in length and is due, in large part, to spatiotemporal variations of the sun's magnetic field. One measurement of solar activity is the number of observable sunspots, which are regions of intense magnetic activity that can produce a sudden release of energy in the form of solar flares and/or coronal mass ejections. In either event, large amounts of electrons, ions, and atoms are projected off of the sun's surface. Once these particles reach earth, they stress the earth's magnetosphere, resulting in changes to the strength and orientation of its magnetic field. As the field changes, some of the charged solar particles can enter the earth's ionosphere, changing the ionospheric current and the magnetic field it produces. As the time-varying magnetic field links conducting loops on the earth's surface, such as electrical transmission circuits, railways, or piping systems, the magnetic field induces an electromotive force (emf) around the loops as dictated by Faraday's law. These geoelectric emfs then drive GICs in the conducting circuits (see Fig. 1).
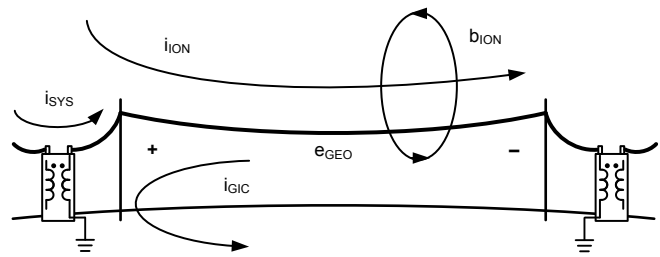

Fig. 1. Creation of GICs: solar storms change ionospheric currents (i_{ION}) and their accompanying magnetic fields (b_{ION}), which induces a geoelectric emf (e_{GEO}) in conducting circuits and generates current flow (i_{GIC}). In the case of electrical circuits, GIC superimposes itself onto the nominal system frequency current (i_{SYS}).

GIC is especially noticeable in high-latitude locations (where the effects of geomagnetic storms are the greatest) and in long, high-voltage lines with tall transmission towers, which results in an increased loop area linked by the magnetic field, and therefore, an increased geoelectric emf.

Because of the slow variation of the induced geoelectric field (relative to the power system frequency), GIC is considered a quasi dc current with frequencies in the millihertz range or lower. Fig. 2 is a capture of the GIC measured in a transformer neutral connection in Finland during a geomagnetic storm that occurred on March 24, 1991 [4]. The current shown has been low-pass filtered to remove any nominal frequency unbalance current that may have been present in the transformer neutral connection. The plot shows the erratic, yet very slowly changing, level of the induced currents. In the middle of the plot, the current maintains a value around –8 A for upwards of 40 minutes. Even during what appears to be a sharp spike to the –200 A level, this transition occurs over roughly 3 minutes, which equates to a frequency of 2.8 mHz. For all practical purposes, these are preexisting dc currents when considering power system frequencies, transients, and even protection-coordinating backup intervals that might be 1 second in length.
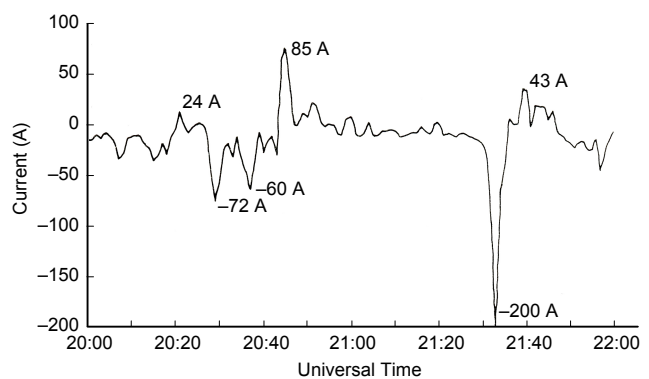

Fig. 2. GIC measured in a transformer neutral connection in Finland during a geomagnetic storm that occurred on March 24, 1991 [4].

When considering the magnitude of GICs, Fig. 2 provides an excellent example of severe GIC levels. In order to indicate their severity, geomagnetic storms are given a K-index rating (which is based on the maximum fluctuations of the earth's magnetic field over a prescribed interval) [5]. The storm that occurred on March 24, 1991 (and that was captured in Fig. 2) was a K-9 level storm, the highest level presently defined. The peak magnitude of 200 A that was captured in Fig. 2 represents an expected worst-case value. However, it is important to remember that this value was measured in the transformer neutral connection and that the GIC present in each phase conductor is essentially one-third of this amount, or 67 A. This per-phase value also agrees with hand calculations of GIC levels in the phase conductors given the magnetic field levels during a large geomagnetic storm and the resistance of a transmission line conductor [6].

Practically, when considering CTs and relays, the GICs are preexisting dc currents with magnitudes that are a small percentage (below 10 percent) of a typical transmission-grade CT's magnitude rating.

III. Simplified CT Model for Protection Considerations

In this section, we review a simplified CT model that is commonly used for protection considerations. This model allows protection engineers to both evaluate the performance of CTs analytically and model CTs using computer simulations. Typical CT performance calculations include sizing a CT for saturation-free operation for a given system (including fault current levels and X/R ratio) and calculating the time-to-saturation for a CT that may saturate (including factoring in the remanent flux in the CT). Typical computer simulations include evaluating the response of a specific relay or protection algorithm to events with saturated CTs.

A. First Principles of CT Operation

A CT is a system with the primary current as an independent input, the secondary current as the output of interest, the burden, and the magnetic core all intertwined with the applicable laws of physics. The first approximation of this system, sufficient for protection studies, is as follows.

The primary (i_1) and secondary (i_2) currents follow the ampere-turn balance equation, with the excitation current (i_μ) modeling the core excitation and saturation. Typically, we have a single primary turn, and N secondary turns; therefore, we can write the following equation:

$$i_1 = N \bullet \left(i_\mu + i_2 \right) \tag{1}$$

We introduce the primary ratio current (i_1') for convenience:

$$i_1' = \frac{1}{N} i_1 \tag{2}$$

So, we can write (1) in secondary amperes as follows:

$$i_1' = i_\mu + i_2 \quad \text{or} \quad i_2 = i_1' - i_\mu \tag{3}$$

Equation (3) signifies that the secondary current equals the primary ratio current less the excitation current. Therefore, the excitation current represents the CT error.

Next, we will tie together the secondary current and the secondary or excitation voltage (v_2). The CT burden links together the secondary current and secondary voltage. Assuming a resistive burden (R_B), typical for microprocessor-based relays, we can write the following equation:

$$v_2 = R_B \bullet i_2 \tag{4}$$

The burden resistance in (4) includes the secondary winding resistance, the CT leads' resistance, and the relay input resistance. Therefore, we can treat the secondary voltage as the excitation voltage for the CT core.

The excitation voltage induced is proportional to the rate-of-change of the magnetic flux; therefore, the magnetic flux linkage (λ) is an integral of the excitation voltage:

$$\lambda = \int v_2 \, dt \tag{5}$$

Finally, we recognize the nonlinear relationship between the flux linkage and the excitation current and can write the following equation:

$$i_\mu = h(\lambda) \tag{6}$$

where h is the nonlinear function representing a relationship between the instantaneous excitation current and the instantaneous magnetic flux linkage. As such, the function h is independent of frequency, at least in the bandwidth of up to a few kilohertz. In general, the function h includes the phenomenon of hysteresis, but we will neglect it here. As we prove later in this paper, hysteresis is not consequential in our simplified CT model for the discussion of the effect of GICs on CT performance.

Equations (1) through (6) are the first principles of a CT. We show them graphically in Fig. 3 using both the circuit model and the signal model.
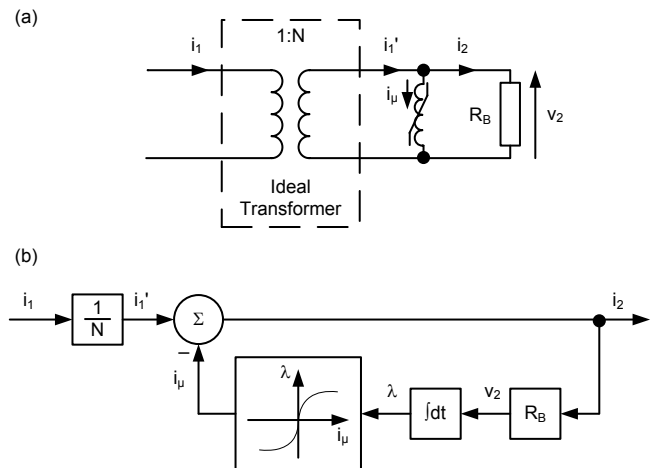

Fig. 3. CT representation using a circuit model (a) and a signal model (b).

The signal model is helpful to better understand the CT operation. Specifically, we can think of the system in Fig. 3b as follows:

- The secondary current (i_2) multiplied by the burden resistance (R_B) creates the secondary voltage (v_2).
- The secondary voltage (v_2) integrated over time produces the flux linkage (λ).
- The flux linkage dictates how much excitation current (i_μ) is drawn by the core based on the nonlinear function h.
- The excitation current controls the value of the secondary current as it subtracts from the primary ratio current (the feedback loop).

The CT representation in Fig. 3b is helpful to understand how CT errors are introduced in the first place. For small primary currents, the feedback in the form of the excitation current is small, making the secondary current practically equal to the primary ratio current. The higher the current, the higher the burden, and/or the lower the frequency, the larger the feedback and the resulting CT errors.

If we combine (5) and (6), we realize that the excitation current is a function of the secondary voltage:

$$i_\mu = h\left(\int v_2 \, dt\right) \qquad (7)$$

Equation (7) leads us to the excitation characteristic of the CT core. As per standard practice, we obtain the excitation characteristic by applying a sinusoidal secondary voltage at the rated frequency (f) and we measure the excitation current. Normally, the true rms of the excitation current is measured during the excitation test (remember that the excitation current is distorted). From the excitation test, we obtain the excitation curve, i.e., the relationship between the excitation voltage (rms of the voltage sinewave) and the excitation current (rms of the distorted current):

$$I_{\mu RMS} = h_{EXC}\left(V_{2RMS}\right) \qquad (8)$$

Relationship (8), obtained experimentally, is the standard way of characterizing the nonlinear nature of the CT core. This curve is published in the CT data sheet and can be verified using simple test equipment. The two functions h_{EXC} (published CT data) and h (element of the CT model) are not the same because h is based on the instantaneous values, not the rms of periodic signals.

B. Frequency Dependence of the CT Characteristic

We have to remember that the excitation curve (8) applies to a given frequency. If measured at a different frequency, the excitation curve is different. Fig. 4 illustrates the frequency dependence of the CT excitation characteristic.
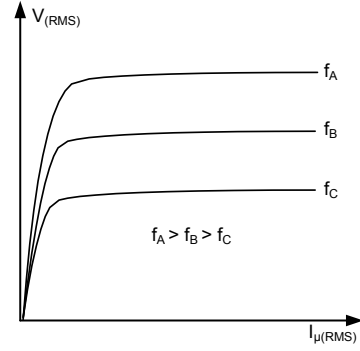

Fig. 4. CT excitation characteristic dependence on frequency.

In order for us to use the model of Fig. 3b and continue with the analysis of CT performance for low frequencies (including GICs), we need to reconcile the frequency dependence shown in Fig. 4 with our model of Fig. 3b.

The flux linkage is an integral of the voltage as per (5). During the excitation test, we apply a sine wave voltage:

$$v_2(t) = V_2 \bullet \sin(2\pi ft) \qquad (9)$$

This voltage results in a sinusoidal flux linkage per (5) as follows:

$$\lambda(t) = \int v_2(t) \, dt = \frac{V_2}{2\pi f} \bullet \sin\left(2\pi ft - \frac{\pi}{2}\right) \qquad (10)$$

We now consider the peak values of the flux linkage (10) for two different frequencies (f_A and f_B) and two different excitation voltages (V_{2A} and V_{2B}) so that the peak flux linkage in both cases is the same (i.e., the resulting peak excitation current is the same):

$$\lambda_{PEAK} = \frac{V_{2A}}{2\pi f_A} = \frac{V_{2B}}{2\pi f_B} \qquad (11)$$

We can rewrite (11) to make the main point clear:

$$\frac{V_{2A}}{f_A} = \frac{V_{2B}}{f_B} \qquad (12)$$

Equation (12) means that when reducing the frequency, we need to reduce the excitation voltage proportionally to keep the excitation current the same (i.e., keep the CT errors the same).

Equation (12) is therefore our basis for frequency derating of a CT (e.g., it tells us that at half of the rated frequency, the CT can measure half of the rated current with the same error and burden). We can better understand (12) by noticing its units: volts per hertz (V/Hz) or volt seconds (Vs), which are the units for flux linkage. Equation (12) is simply a constant flux linkage equation or a constant V/Hz equation.

Importantly, we can model this frequency dependence of the CT with a single frequency-independent characteristic, h, in our model of Fig. 3b. Lower signal frequency means that the integral of the voltage (the area under the voltage wave shape) becomes larger. This integral is the flux linkage. Therefore, the lower the frequency, the higher the peak flux linkage and the higher the excitation current for the same peak secondary voltage. From (9) and (10), we obtain the frequency dependence as shown in Fig. 4 with a single, frequency-independent function, h, in our model

C. Sample CT for Laboratory Tests

We now illustrate the performance of the model shown in Fig. 3b using the data of a sample C10, 150:5 CT (shown in Fig. 5). We used a shunt to measure the primary current as a reference for CT accuracy and to obtain the input to our CT model. A shunt is a resistor of negligible, yet precise, ohmic value, which allows for accurate current measurements by measuring the proportional voltage signal across the shunt. In our setup, we fed the voltage signal into an isolator amplifier, which boosted the voltage to the appropriate level for our recording device. We used a second shunt to measure the secondary current. The true benefit of using shunts to measure the current was that doing so allowed us to accurately measure alternating current (ac) and dc current together without any concern of saturation in our measurement equipment. We precisely recorded the primary current flowing through the CT and the secondary current produced by the CT. We used multiple primary turns so that we could apply lower currents from a relay test set and still achieve the rated ampere-turn levels in the tested CT. In all of the examples that follow, we show the equivalent primary current as if a single primary turn was used. We measured the total secondary resistance with a dc ohmmeter to be 87 mΩ. Finally, we obtained the excitation characteristic for the CT via testing, as shown in Fig. 6.
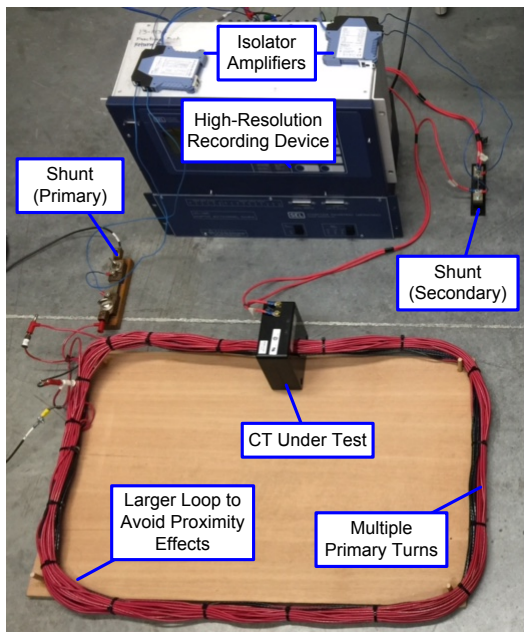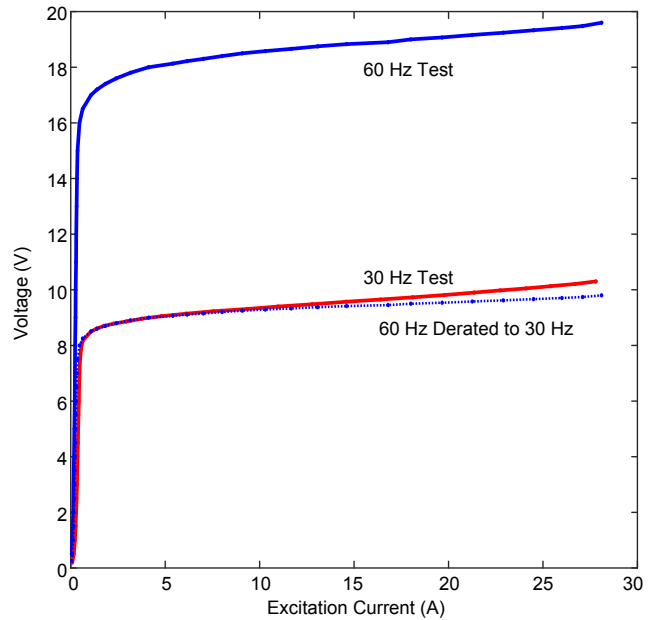

Fig. 5.   The C10, 150:5 CT under test.

Fig. 6.   Excitation characteristic of the sample CT: 60 Hz test, 30 Hz test, and the 60 Hz curve derated to 30 Hz frequency.

Per standard practice, we plot the excitation curves of Fig. 6 for rms values of the sinusoidal voltage and rms values of the excitation current. The current is distorted, especially in the saturation region of the curve. Fig. 7 illustrates this distortion by plotting both the rms and the peak values of the excitation current.
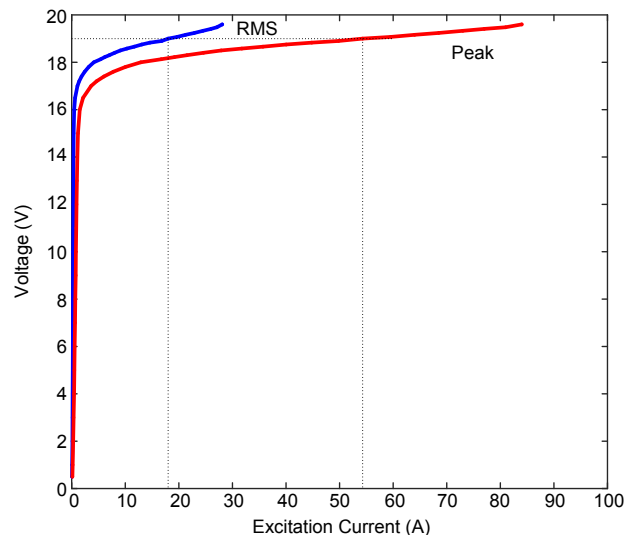

Fig. 7.   Excitation characteristic (60 Hz) of the sample CT: the true rms and peak excitation current.

Consider a sample point of 19 V rms. At this voltage, the true rms value of the excitation current is about 18 A, while the peak value of the excitation current is about 54 A. The higher the voltage, the larger the difference between the rms and the peak values of the current.

Per standard practice, we characterize CTs by plotting the rms excitation curve, h_{EXC}. Therefore, before we can use the model of Fig. 3b, we need to derive the function h in (6) from the measured excitation curve. We do this by simulating the excitation test in the model of Fig. 3b and manipulating the

function h until we obtain a good match between the actual (measured) and simulated excitation curves. We can use a linear piece-wise approximation for the function h or fit an analytical expression to the data. In this paper, we used the following analytical expression for the function h for the sample C10, 150:5 CT with the characteristic of Fig. 6:

$$i_\mu = 9.04\lambda + 0.0888\left(\frac{\lambda}{0.0563}\right)^{27} \qquad (13)$$

In (13), the flux linkage is in secondary volt seconds and the current is in secondary amperes. Fig. 8 compares the relationship between the excitation characteristic h_{EXC} and the function h. For ease of comparison, we scaled the function h in Fig. 8 from volt peak seconds to volts rms. We can see that the shape of the function h is similar to the measured excitation curve, but the two are not identical. We can also observe that the function h is relatively close to the excitation characteristic measured for the peak excitation current. Deriving the function h, including hysteresis, from the standard excitation curve belongs to the art and science of CT simulation, and is outside the scope of this paper.
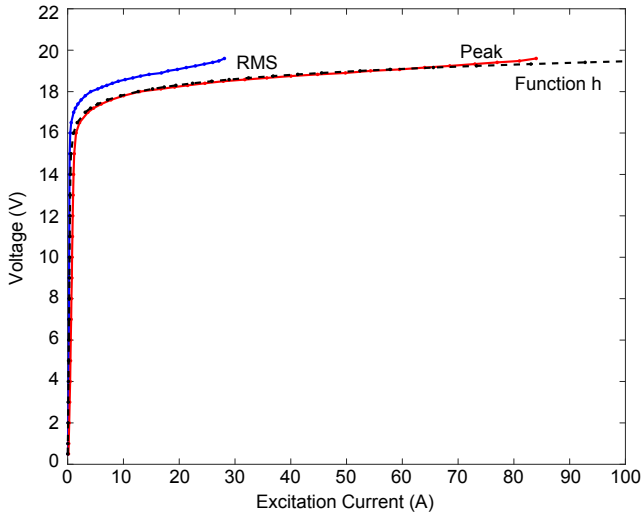

Fig. 8. Excitation characteristic (60 Hz) of the sample CT: measured excitation curves and best-fit function h (dashed) modeling the CT.

Fig. 9 compares the measured excitation curves at 60 Hz and 30 Hz with the excitation curves obtained from the model of Fig. 3b using the h function derived to match the 60 Hz curve and shown in Fig. 8. Note that both the 60 Hz and 30 Hz curves match well. This proves the point that a single frequency-independent function h models the CT reasonably well for different frequencies.
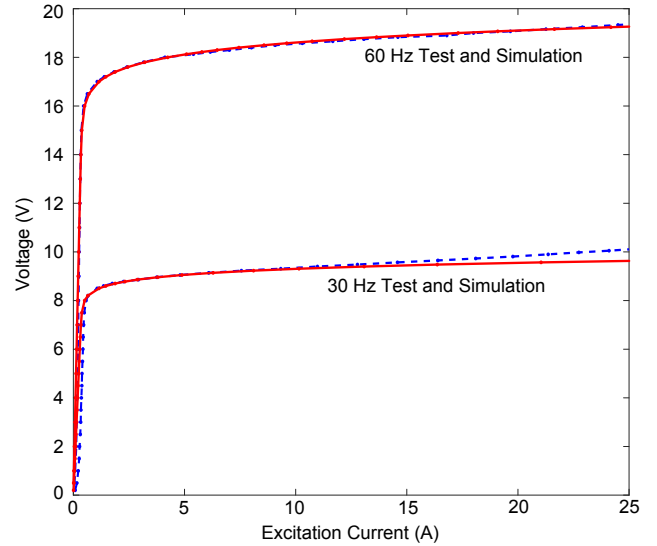

Fig. 9. Comparison of measured (blue dashed) and simulated (red) excitation curves for the sample CT at 60 Hz and 30 Hz.

D. Illustration Examples

Having the model of Fig. 3b matched to our physical CT, we now illustrate the response of the CT and the accuracy of our simple model for a typical fault current with a decaying dc offset at two different frequencies.

1) Example 1

First, we show an example of an offset fault current with the decaying dc component having a 30 ms time constant and a magnitude of 1,350 A rms primary (9 times rated and the maximum capacity of our laboratory equipment) at 60 Hz. Fig. 10 shows the primary ratio current, the secondary current, and the excitation current recorded for the CT in our laboratory. Fig. 11 shows the same signals, the secondary voltage, and the flux linkage obtained from the model of Fig. 3b, with the h function matching the 60 Hz excitation curve and given by (13).

In this example, the CT is transiently saturated due to the decaying dc offset, which brings the flux linkage (integral of the secondary voltage) above the knee-point of the excitation characteristic. Once the dc offset decays, the CT pulls out of saturation because the flux linkage decays below the knee-point and only a small excitation current is drawn (we explain this phenomenon in detail in Section VI).
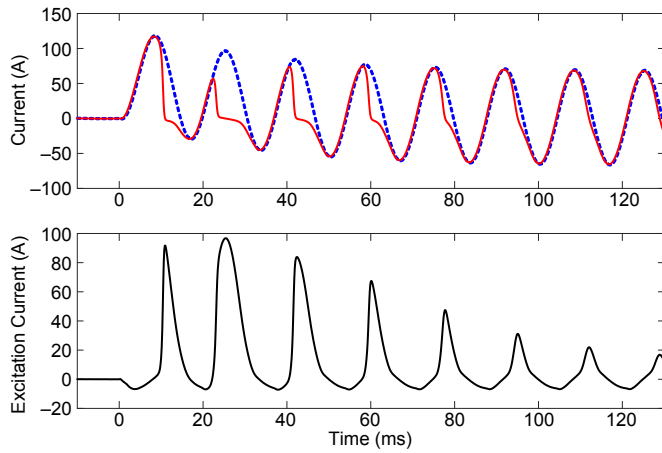
Fig. 10. Example 1 (laboratory test): primary ratio current (blue dashed), secondary current (red), and excitation current.
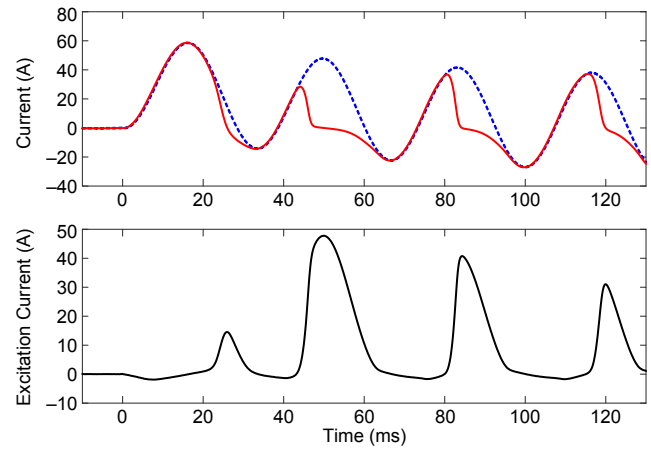

Fig. 12. Example 2 (laboratory test): primary ratio current (blue dashed), secondary current (red), and excitation current.
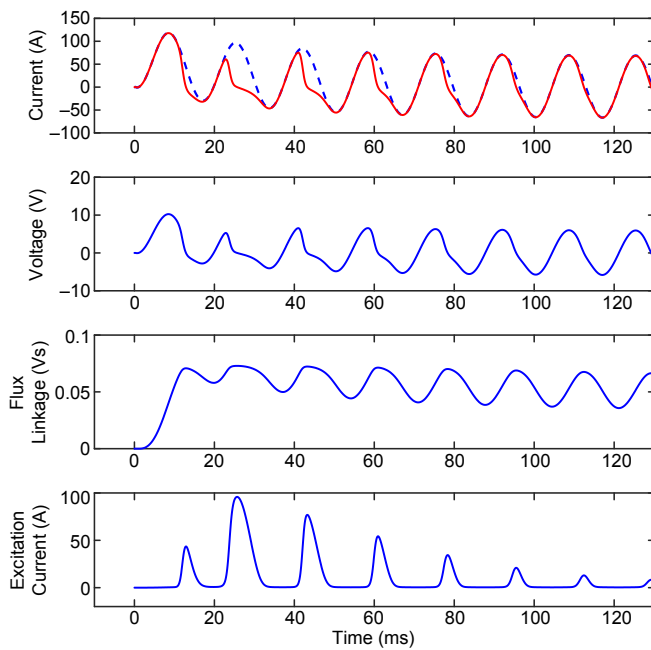

Fig. 11. Example 1 (computer simulation): primary ratio current (blue dashed), secondary current (red), secondary voltage, flux linkage, and excitation current.
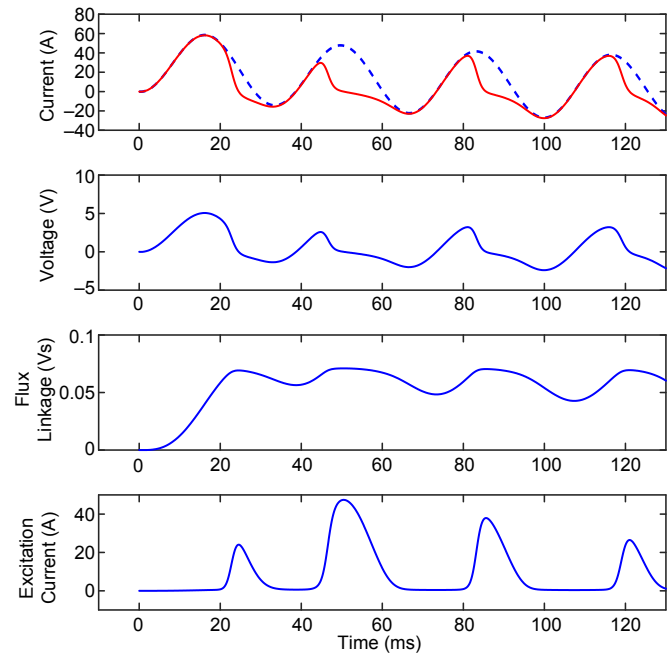

Fig. 13. Example 2 (computer simulation): primary ratio current (blue dashed), secondary current (red), secondary voltage, flux linkage, and excitation current.

2) Example 2

In this example, the current is 30 Hz and the dc time constant is 60 ms. We halved the current magnitude (i.e., used 4.5 times rated or 675 A rms primary). Fig. 12 shows the test results, while Fig. 13 shows the simulation results.

Note that the responses in Fig. 10 and Fig. 12 are very similar. This illustrates our main point about frequency derating: the lower the frequency, the lower the current that can be measured by the CT with the same error. If we upscale the time axis by the factor of two, we need to downscale the current axis by a factor of two in order to keep the flux linkage and excitation currents at the same level. The two examples also demonstrate that our simple CT model represents the actual CT reasonably well.

In this section, we reviewed a simple CT model capable of representing a CT for decaying dc offset present in fault currents, as well as for off-nominal frequencies of the ac component. Next, we apply this model to situations with very low-frequency current before moving on to situations with dc current representative of GICs in power systems.

IV. CT RESPONSE TO CURRENT WITH MULTIPLE FREQUENCY COMPONENTS

In the previous section, we noted that frequency has a dramatic impact on the maximum current magnitude that can be reproduced by a CT with negligible errors. Equation (12) specifies the frequency derating rule. A two-fold reduction in frequency corresponds to a two-fold reduction of the knee-point voltage, or in other words, a two-fold reduction in the magnitude of the current reproduced with the same errors.

A. CT Response to a Very Low-Frequency Current

We illustrate this phenomenon by applying a very low-frequency (0.2 Hz) current to our sample 150:5 CT. Under the rated burden, this CT works very well for the rated current of 150 A rms, 60 Hz and does not saturate for 20 times the rated current (i.e., it can measure up to 3 kA rms of current at 60 Hz without saturation). At 0.2 Hz, however, the no-saturation current level is only 3,000 • 0.2 / 60 = 10 A rms [see (12)]. If we subject this CT to 150 A rms current at 0.2 Hz, we expect it to saturate.

Fig. 14 shows the primary ratio, secondary, and excitation currents measured in our laboratory. Fig. 15 shows the response of our simple model to this particular test condition. Our model reproduces the case of very low-frequency current reasonably well.
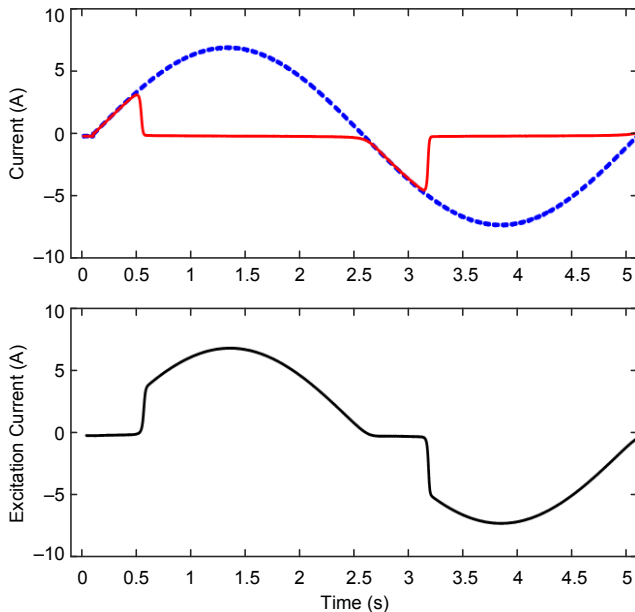
Fig. 14.   Response of the sample CT to a 0.2 Hz, 150 A rms current (laboratory test): primary ratio current (blue dashed), secondary current (red), and excitation current.
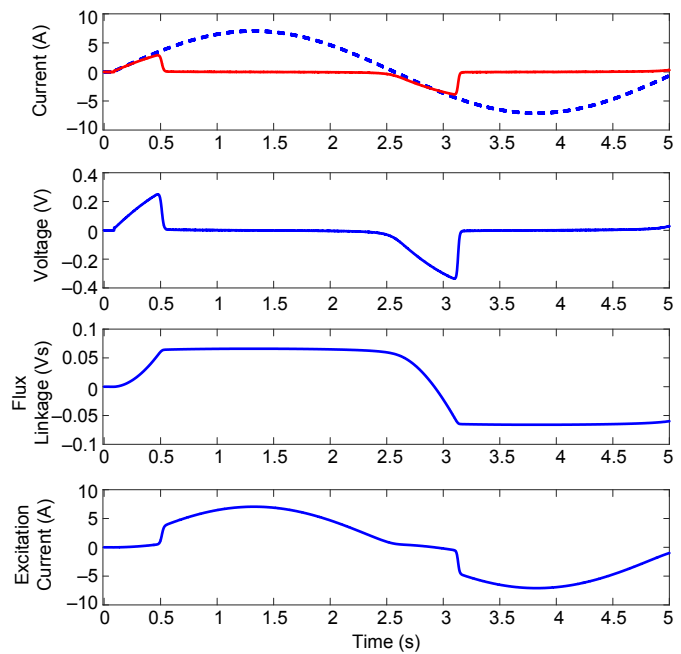
Fig. 15.   Response of the sample CT to a 0.2 Hz, 150 A rms current (computer simulation): primary ratio current (blue dashed), secondary current (red), secondary voltage, flux linkage, and excitation current.

We see that the CT is deeply saturated for long periods of time. The secondary current drops to zero in 0.5 seconds and stays zero for the rest of the half cycle (i.e., for the next 2 seconds). Fig. 15 explains why: the low-frequency current produces voltage across the burden resistor that is unipolar for the duration of half of a cycle (2.5 seconds). When integrated, this unipolar voltage makes the flux linkage increase all the way to the saturation level. When the flux linkage reaches the saturation level, the entire ratio current closes via the excitation branch and the secondary current is very small (practically zero). The CT is "completely saturated."

If this very low-frequency current represented a GIC current, we might suspect that the CT would not reproduce the 60 Hz current at all, leading to serious problems for protection. To check this hypothesis, we tested a case of two signal frequencies superimposed in the primary current.

B. CT Response to a Current Containing Very Low-Frequency and Nominal Frequency Components

We now apply the low-frequency 0.2 Hz, 150 A rms current from the previous test but add a 60 Hz, 150 A rms (rated) component to the primary current. We have shown that the 0.2 Hz component on its own completely saturates the CT, while the 60 Hz component on its own is reproduced well. What are we going to measure in the CT secondary winding with both current components applied at the same time?

Fig. 16 presents the laboratory test results, while Fig. 17 presents the results of computer simulations for this test condition. Our simulation results match the laboratory tests.
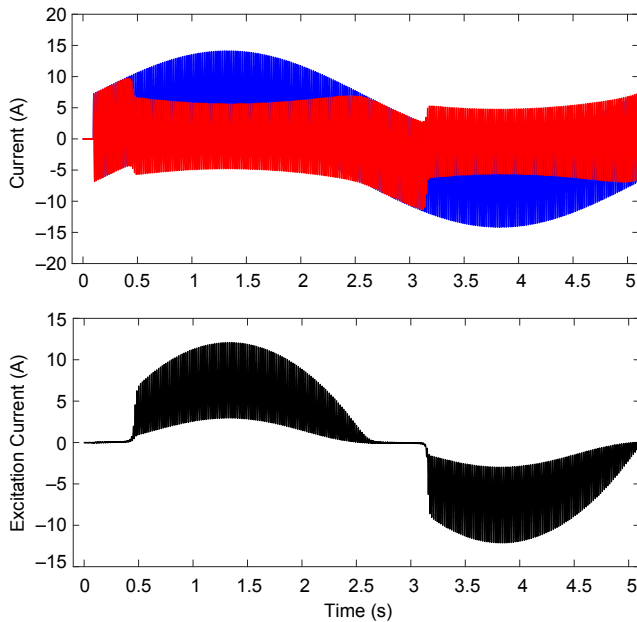
Fig. 16.   Response of the sample CT to a 0.2 Hz, 150 A current superimposed on the 60 Hz, 150 A current (laboratory test): primary ratio current (blue), secondary current (red), and excitation current.
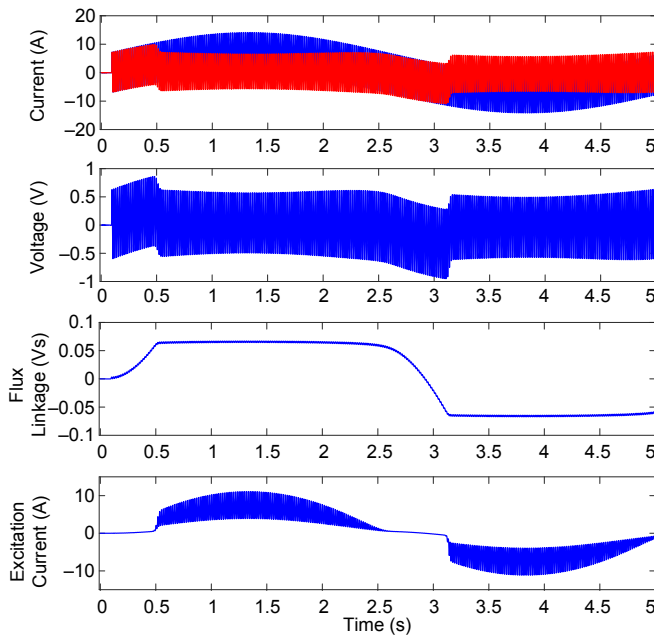

Fig. 17.   Response of the sample CT to a 0.2 Hz, 150 A current superimposed on the 60 Hz, 150 A current (computer simulation): primary ratio current (blue), secondary current (red), secondary voltage, flux linkage, and excitation current.

What is interesting about the result is that while the 0.2 Hz component is reproduced poorly with extremely deep saturation lasting 2 seconds in each half cycle of the 0.2 Hz component, the 60 Hz current component is reproduced relatively well by the CT.

To check the errors for the 60 Hz component, we filtered the primary ratio current and the secondary current of Fig. 16 with a band-pass filter tuned to 60 Hz and plotted the filtered currents in Fig. 18. As we can see from the figure, the magnitude and phase angle errors are moderate (27 percent

and 39 degrees maximum, respectively), despite the fact that the low-frequency component is as high as the rated current.
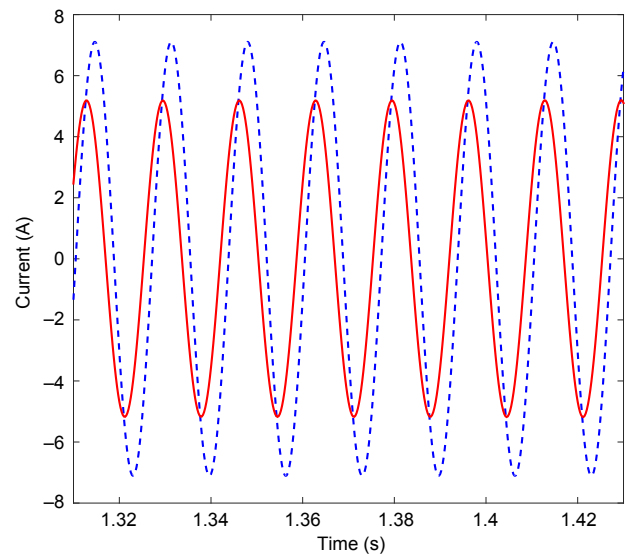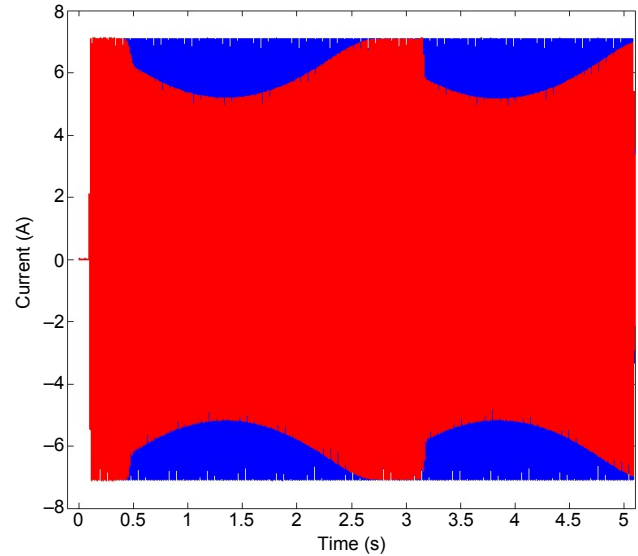

Fig. 18.   Band-pass filtered 60 Hz components in the primary ratio current (blue dashed) and secondary current (red) for the case of Fig. 16.

The simple tests presented in this section demonstrate that the CT can be simultaneously saturated for the low-frequency current component and not saturated or a little saturated for the rated frequency current component. How is this possible? We will explain this phenomenon after reviewing test results with a strict dc component.

V. CT RESPONSE TO DC CURRENT

GICs change very slowly. We can approximate them better with a dc component than with a very low-frequency ac component. In this section, we show the results of tests similar to those of Section IV, but we use dc current to represent the effect of GIC.

A. CT Response to DC

Being a transformer, a CT does not reproduce a dc component in the steady state. However, according to our CT model of Fig. 3b, a dc component flows initially to the secondary winding. This dc component creates a dc excitation voltage through the voltage drop across the burden resistance. This voltage is integrated into a flux linkage, and therefore, the flux linkage ramps up linearly until it causes the excitation current to be equal to the primary ratio current. At that point, the CT reaches an equilibrium steady state in which the excitation current equals the primary ratio dc current, and as a result, the secondary current equals zero. Fig. 19 illustrates the response of the model from Fig. 3b for the primary current of 150 A dc (5 A dc secondary). Note that it takes some time for the flux linkage to build up to the equilibrium point. The higher the dc and the higher the CT burden, the higher the excitation voltage. The higher the excitation voltage, the higher the rate of rise of its integral (i.e., the flux linkage).
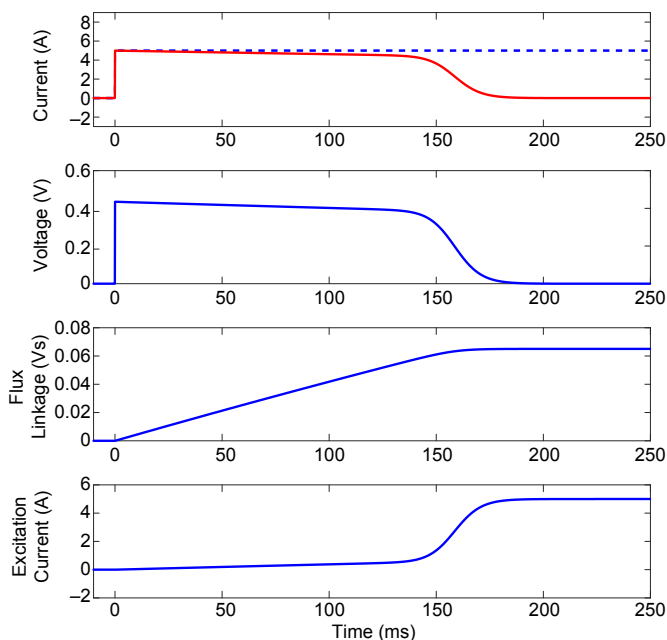

Fig. 19.   Response of the sample CT model to a dc current of 150 A (computer simulation): primary ratio current (blue dashed), secondary current (red), secondary voltage, flux linkage, and excitation current.

Note that the CT equilibrium point is defined by the excitation current of 5 A secondary and the flux linkage of 0.065 Vs. Fig. 20 shows the equilibrium point on the CT characteristic h.
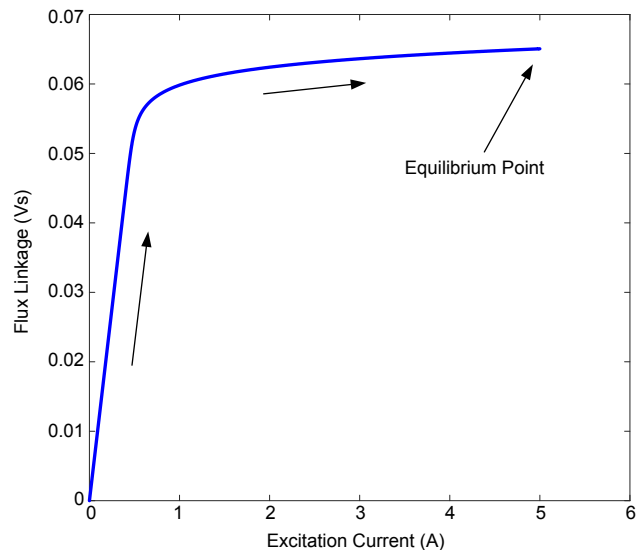

Fig. 20.   Response of the CT model to a dc current of 150 A: equilibrium point on the flux linkage excitation current characteristic h.

We verified the simulation by applying dc to the physical CT in our laboratory. Fig. 21 shows the results and confirms an agreement between our model and the physical CT. We attribute the difference in the saturation time (140 ms in the model versus 120 ms in the laboratory test) to the finite accuracy of the excitation characteristic in our model.
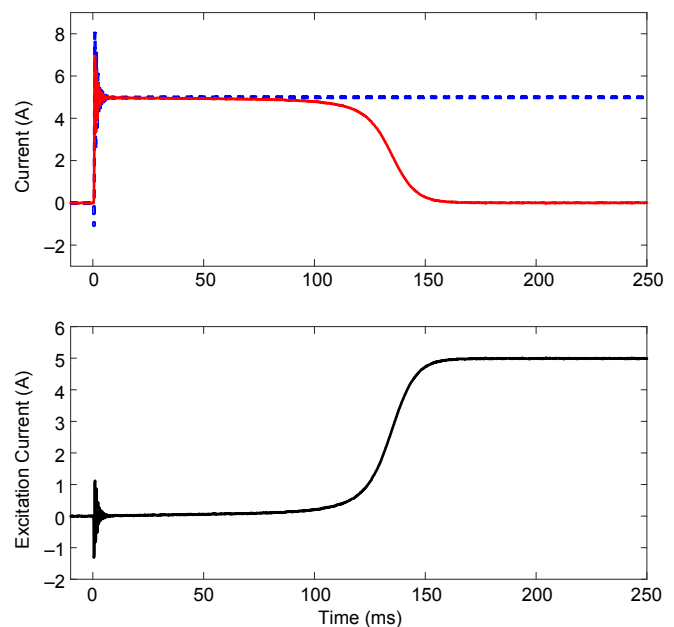

Fig. 21.   Response of the CT model to a dc current of 150 A (laboratory test): primary ratio current (blue dashed), secondary current (red), and excitation current.

The CT response depicted in Fig. 19 and Fig. 21 resembles a pattern often seen in generator CTs for remote fault currents. The generator CTs reproduce the long-lasting, exponentially decaying dc component caused by the large X/R ratio for some time. After that time, the exponentially decaying dc component in the secondary currents collapses rapidly. We see the same pattern here, and the rapid collapse of the secondary current occurs when the flux linkage crosses the knee-point of

the CT characteristic, drawing increasingly higher excitation current.

For illustration, we use the CT model of Fig. 3b and mark it up with the steady-state values for the case of dc in the primary current (Fig. 22). We will return to Fig. 22 when we consider the superposition of the dc and ac components in the primary current.
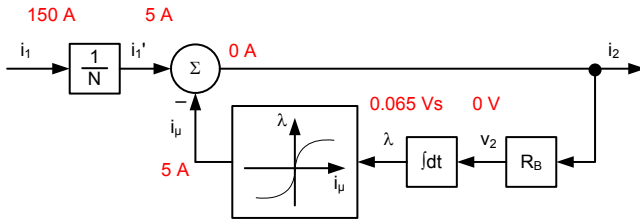

Fig. 22.   Steady-state values in the simplified CT model for the case of dc primary current.

B. CT Response to a Combination of DC and AC Currents

From the previous subsection, we can say that the CT is completely saturated with the dc component. However, we now examine what happens if we subject the CT to the combination of the dc and ac components. We use the sample C10 CT with the currents of 150 A dc and 150 A ac at 60 Hz. Fig. 23 shows the simulation results, and Fig. 24 shows the laboratory test results.
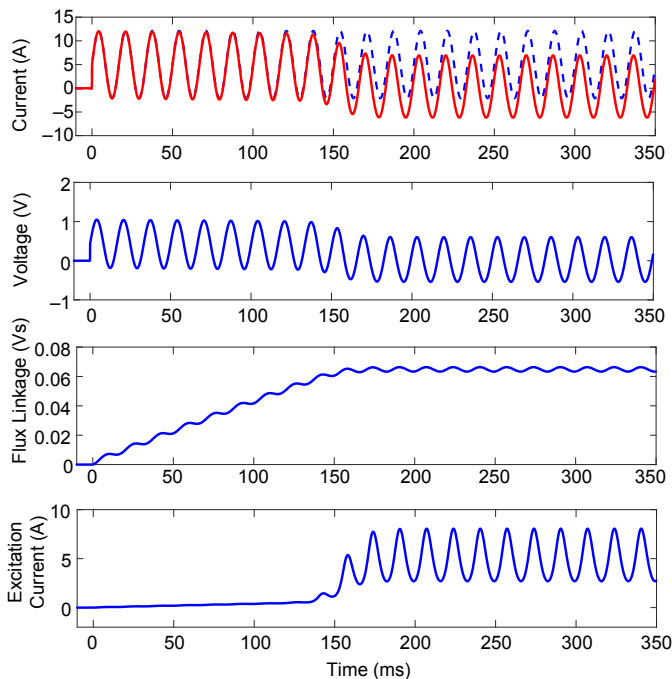

Fig. 23.   Response of the sample CT to a dc current of 150 A and an ac current of 150 A rms (computer simulation): primary ratio current (blue dashed), secondary current (red), secondary voltage, flux linkage, and excitation current.
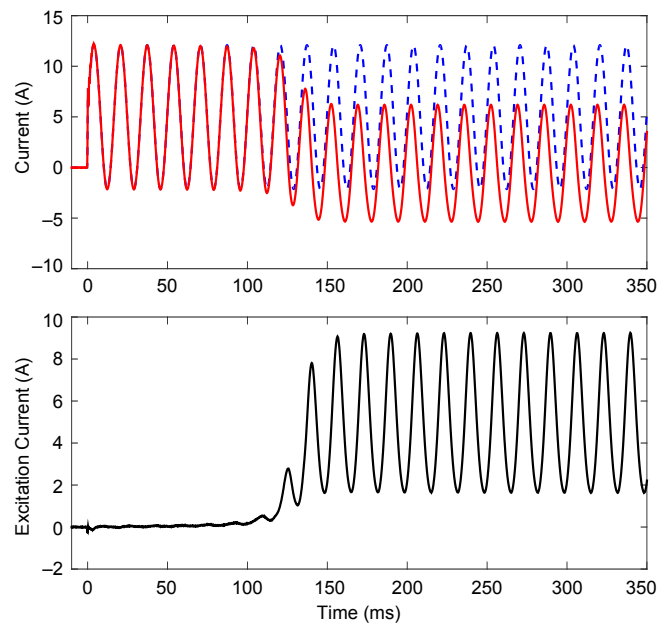

Fig. 24.   Response of the sample CT to a dc current of 150 A and an ac current of 150 A rms (laboratory test): primary ratio current (blue dashed), secondary current (red), and excitation current.

As expected from Section IV, we see that the dc component in the secondary current begins to disappear after some time (140 ms in the model and 120 ms in the laboratory test) because the dc-driven flux linkage reached the saturation level. However, the ac component is reproduced relatively well. We filter the primary and secondary currents of Fig. 24 with a band-pass filter tuned to 60 Hz to measure the accuracy of the CT for the 60 Hz signal (Fig. 25). We conclude that the CT reproduces the 60 Hz signal with a 19 percent magnitude error and a 31 degree phase error.
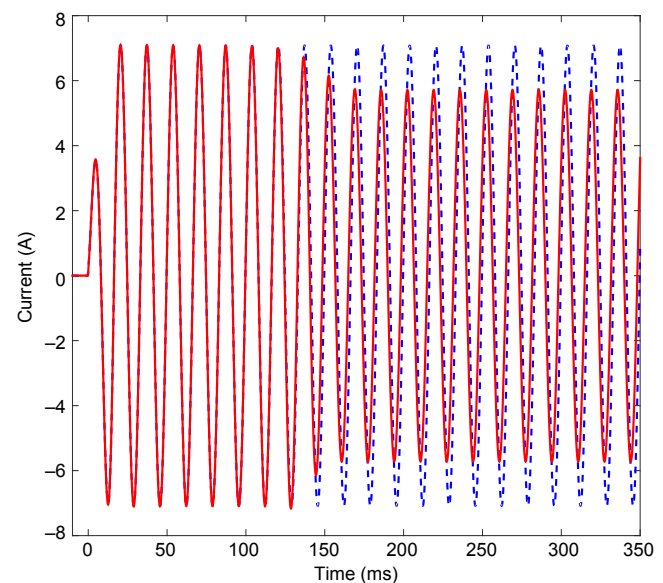

Fig. 25.   Band-pass filtered 60 Hz components in the primary ratio current (blue dashed) and secondary current (red) for the case of Fig. 24.

We can explain the results by realizing that the 150 A rms primary ac current (5 A rms secondary) produces only 5 A • $\sqrt{2}$ • 0.087 Ω = 0.61 V peak ac excitation voltage. At 60 Hz, this voltage corresponds to only 0.61 V/(2 • π • 60) = 0.00162 Vs peak in the flux linkage. From Fig. 20, we see that the 150 A dc current brings the flux linkage to the equilibrium point of 0.065 Vs. The extra 0.00162 Vs peak oscillatory value superimposed around this bias of 0.065 Vs is very small (about 2.5 percent). As a result, the operating point on the flux linkage excitation current plane is able to oscillate around the equilibrium of 5 A (excitation current) and 0.065 Vs (flux linkage) shown in Fig. 20. The steady-state trajectory on the flux linkage excitation current plane is shown in Fig. 26. For this condition, the maximum flux linkage reaches about 0.0665 Vs, which draws an excitation current of about 8 A peak, or about 3 A peak in addition to the 5 A dc bias. The excitation current associated with the 60 Hz component is increased due to the presence of the dc bias but is still relatively low, meaning the CT errors are not very large.
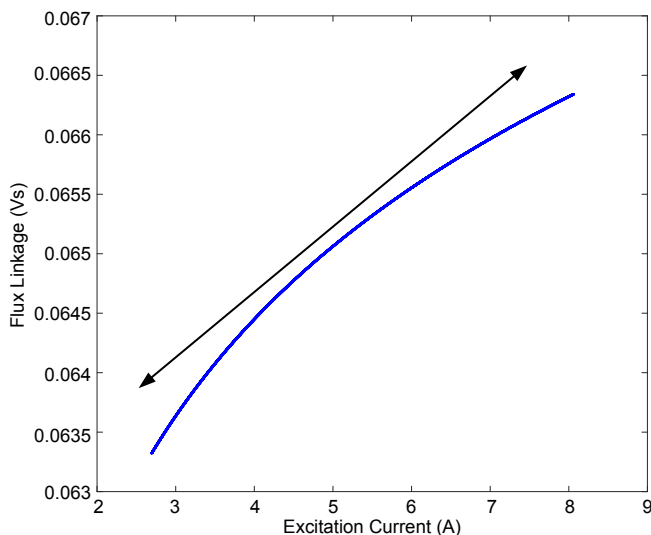

Fig. 26. Response of the sample CT to a dc current of 150 A and an ac current of 150 A rms (computer simulation): steady-state flux linkage excitation current trajectory.

We verified the plot of Fig. 26 using laboratory test data by calculating the secondary voltage from the recorded secondary current using the burden resistance and integrating it to obtain the flux linkage. Next, we calculated the excitation current by subtracting the recorded secondary current from the recorded primary current scaled by the ratio. Fig. 27 shows the results. The trajectories of Fig. 26 and Fig. 27 agree. In the case of the actual CT, we see the hysteresis loop as expected. Our simplified model does not include the hysteresis, hence the difference in kind.

The above simulations and tests confirm that the dc component creates a bias in the model of the CT, as illustrated in Fig. 22. The ac component creates an oscillation around this bias point. This increases the excitation current compared with no dc present, but the difference is not as dramatic as one might expect. This observation is also a key finding in [3].
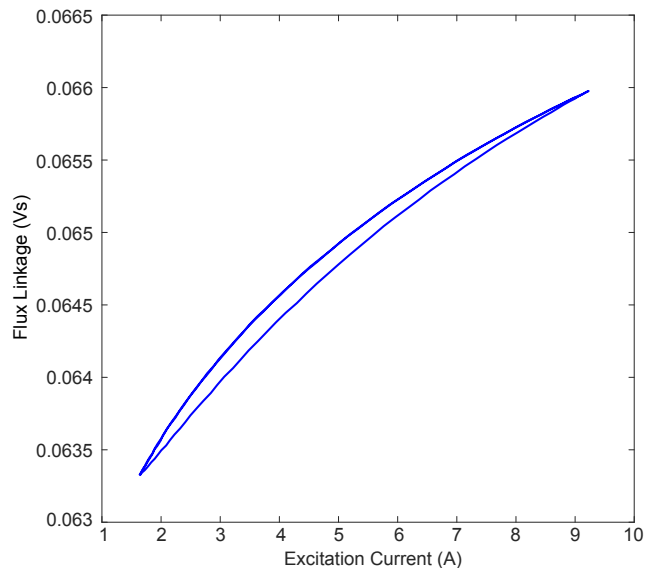

Fig. 27. Response of the sample CT to a dc current of 150 A and an ac current of 150 A rms (laboratory test): steady-state flux linkage excitation current trajectory.

VI. CT PERFORMANCE FOR FAULT CURRENTS WITH GIC

A. Fault Current Examples

Our previous examples assumed that the dc component was equal to the rated current of the CT. In practice, a GIC component is in the range of 10 percent or less of the CT rated current. For example, a 50 A dc per-phase current in a transmission line protected using 800/5 CTs is only 50 / 800 = 6.25 percent of the rated current. This low bias impacts CT performance under fault conditions, but to a very small degree.

For illustration, consider the following scenario for our sample C10, 150:5 CT:

- Preexisting dc component of 10 percent of rated (15 A dc).
- Preexisting load (prefault) current of 100 percent of rated (150 A rms).
- Fault current of 20 times rated (3 kA rms).
- The burden of 0.1941 Ω in order to obtain 10 percent steady-state error at exactly 20 times the rated current.

Fig. 28 and Fig. 29 show our simulation results without and with the dc component, respectively. Of course, the dc component itself is not reproduced by the CT. In the steady state, the ac component is reproduced well in both cases (with and without the small dc component present). However, the response in the first half cycle of the fault is quite different. The standing dc component of 10 percent of rated (i.e., 0.5 A dc secondary) offsets the flux linkage value by about 0.053 Vs [compare with the function h in (13)]. This value is significant compared with the knee-point flux linkage and causes saturation if the fault current's first half-cycle polarity is the same as the standing dc current. The CT then pulls out of saturation (we explain this phenomenon in detail later in this section), and in steady state, the variation in the flux linkage is still happening at the 60 Hz frequency and the secondary

voltage and currents are still reasonably accurate, as dictated by (10) and (7).
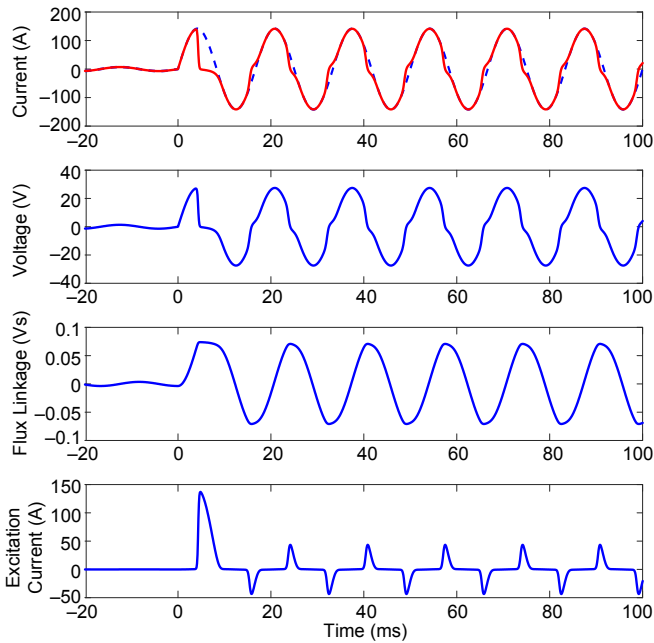

Fig. 28. Response of the sample CT to the fault without a GIC component (computer simulation): primary ratio current (blue dashed), secondary current (red), secondary voltage, flux linkage, and excitation current.
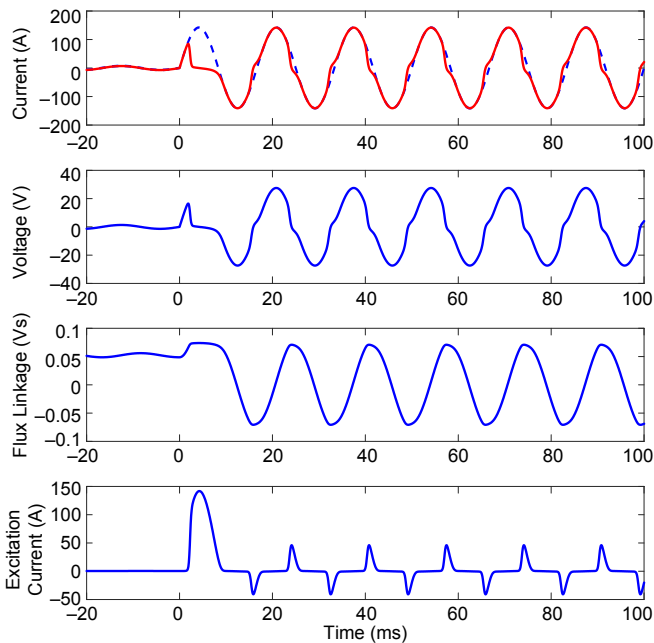

Fig. 29. Response of the sample CT to the fault with a GIC component of 10 percent rated (computer simulation): primary ratio current (blue dashed), secondary current (red), secondary voltage, flux linkage, and excitation current.

We verified the fault current tests with and without a GIC on our physical CT. However, we are not able to drive 3 kA fault currents using our existing test equipment. Fig. 30 and Fig. 31 show test results without and with GIC for the fault current of 1.6 kA, respectively.

The test results agree with our model. Specifically, with GIC present, the CT performance is little affected in the

steady state but is considerably affected in the first half of a cycle of the fault.

Fig. 31 also shows a slightly elevated error for the load current and for the steady-state fault current. However, these errors are minor. The key point illustrated by the test shown in Fig. 30 and Fig. 31 is the significant impact of the very small GIC (10 percent of rated) on the first half cycle of the secondary fault current.

Fig. 30. Response of the sample CT to a fault current of 1.6 kA rms with a prefault load of 150 A rms and no GIC (laboratory test): primary ratio current (blue dashed), secondary current (red), and excitation current.
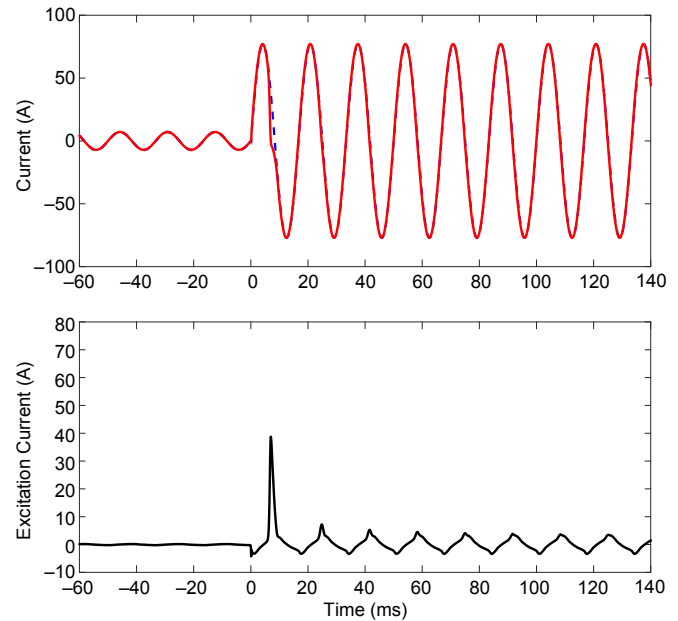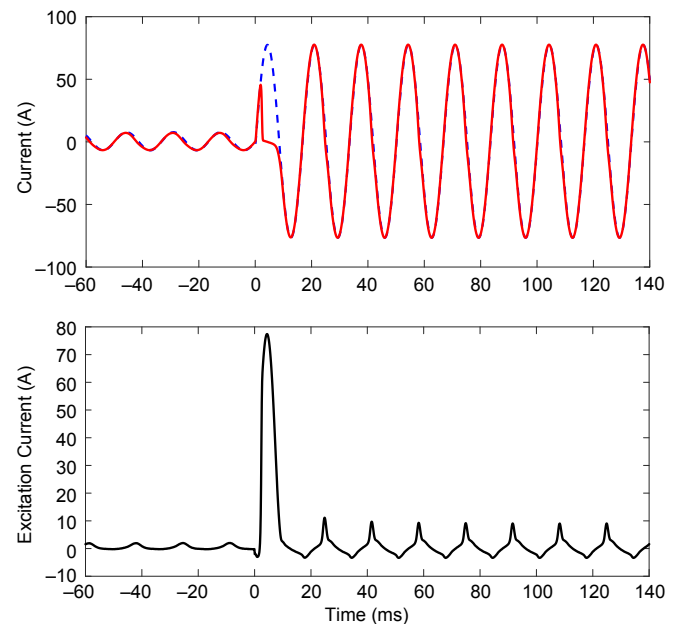

Fig. 31. Response of the sample CT to a fault current of 1.6 kA rms with a prefault load of 150 A rms and with a GIC of 15 A dc (laboratory test): primary ratio current (blue dashed), secondary current (red), and excitation current.

These results are very significant. The small (10 percent of rated) standing dc (GIC) has no significant impact on the

performance of the CT in the steady state. The load current is measured relatively precisely. Similarly, the fault current is reproduced half a cycle into the fault. However, even a small level of standing dc component has a significant impact on the first half cycle of the fault current. The standing current biases the flux linkage considerably. This bias has an effect similar to the remanent flux in the CT core.

B. Explanation of CT Recovering From Transient Saturation

We now explain the impact of remanent flux on CT performance under fault conditions and the mechanism responsible for the recovery from transient CT saturation. We focus on these aspects because we realize that a standing dc component (GIC) has a similar impact as a high-remanent flux.

Fig. 32 shows the performance of our sample CT under an ac current of 10 times rated and the remanent flux linkage of 0.00, 0.01, 0.02, 0.03, and 0.05 Vs. The higher the remanent flux, the more significant the transient saturation (we modeled the remanent flux with the initial value of the integrator's output in the model of Fig. 3b). What is critically important is that the CT recovers from the transient saturation within about half of a cycle.
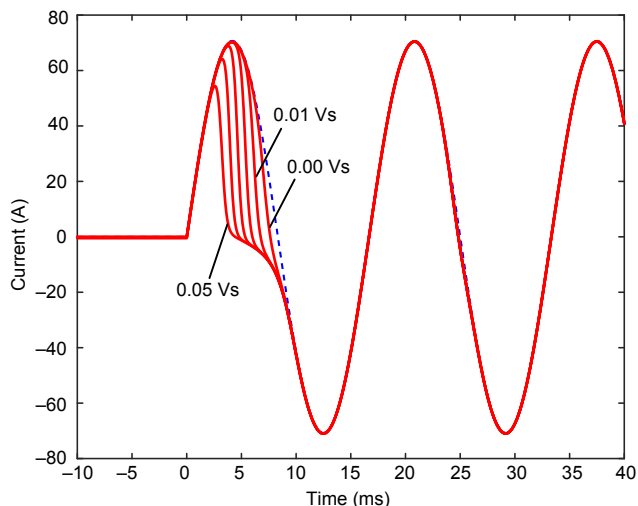

Fig. 32. Response of the sample CT to a fault current of 10 pu rms with remanent flux linkage between 0.00 Vs and 0.05 Vs (computer simulation): primary ratio current (blue dashed) and secondary current (red).

We explain this recovery as follows. Consider Fig. 33, which shows the case of the sample CT with a remanent flux linkage of 0.05 Vs and plots both the secondary current and the flux linkage. When the current is applied, the flux linkage is at 0.05 Vs. The flux linkage increases to about 0.065 Vs and stops increasing further because the CT draws very large excitation current at this level. The voltage is proportional to the secondary current, so the flux linkage increases by a value proportional to Area 1 under the positive quarter of the cycle of the secondary current. Subsequently, the current becomes negative, so the voltage and the flux linkage decrease by a value equal to Area 2. Because Area 2 is considerably greater than Area 1, the flux linkage decreases to well below the initial value of 0.05 Vs. This situation repeats as long as the CT goes into saturation. As a result, the CT has an inherent

tendency to remove transient saturation. In the case of remanent flux linkage and/or GICs, the transient saturation lasts for just above a half cycle.
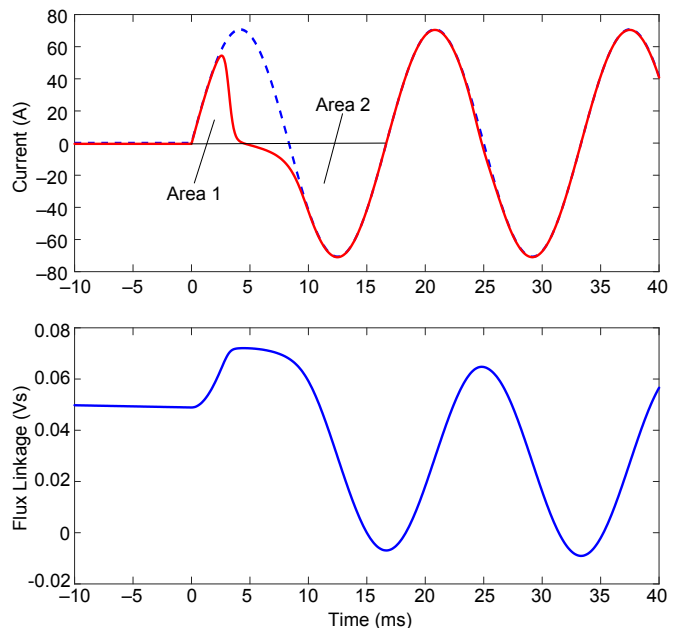

Fig. 33. Response of the sample CT to a fault current of 10 pu rms with a remanent flux linkage of 0.05 Vs (computer simulation): primary ratio current (blue dashed), secondary current (red), and flux linkage.

VII. DERATING CTs FOR GIC

A. Derating for Steady-State Performance

We use our model to derive the first approximation of the CT derating rule for GIC. First we consider steady-state performance. The "no-saturation" CT operating condition is specified by the CT error being below 10 percent. We use the 10 percent difference between the primary ratio current magnitude and the secondary current magnitude as the limit of no-saturation operation. We step through a range of GIC values for our reference CT and find—for each GIC value— the symmetrical ac current that brings us to the 10 percent error. We apply a burden of 0.1941 Ω in order to obtain a 10 percent error at exactly 20 times rated. Table I and Fig. 34 show the results of this experiment.

TABLE I
MAXIMUM AC CURRENT REPRODUCED WITH 10 PERCENT ERROR
FOR A GIVEN DC CURRENT (150:5 CT)

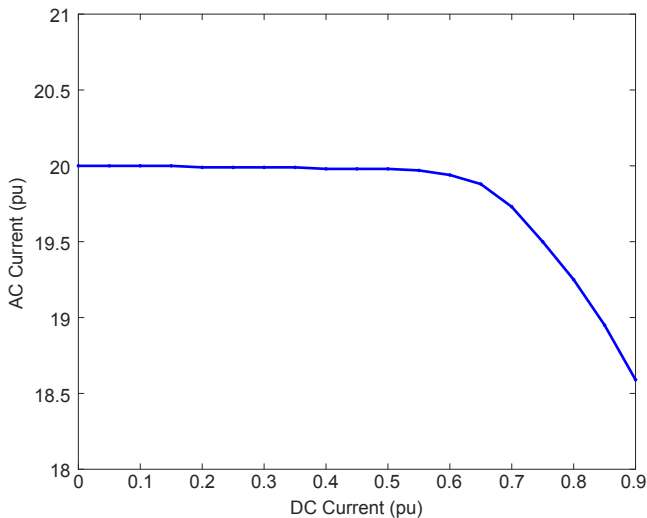| I_{DC} (pu)	I_{AC} (pu)
0	20.00
0.1	20.00
0.2	19.99
0.3	19.99
0.4	19.98
0.5	19.98
0.6	19.94
0.7	19.73
0.8	19.25
0.9	18.59

Fig. 34.   Maximum ac current reproduced with 10 percent error (in per unit of CT nominal) as a function of dc current (in per unit of CT nominal).

Fig. 34 shows us that for relatively small values of the dc current (the case of GIC), the impact is negligible. However, if the amount of dc approaches the CT nominal current, the impact becomes dramatic.

Our results are congruent with the findings of Section V. Small dc currents (practical GIC) cause a negligible effect on steady-state load and the fault performance of CTs.

B. Derating for Transient Performance

As illustrated in Section VI, a standing dc component offsets the flux linkage by the value determined by the excitation characteristic of the core. This offset decreases the room we have to accommodate the fault current without saturation. We offer the following calculations to evaluate the derating factor for the transient CT performance due to GIC.

First, we read the dc voltage component in the excitation voltage from the excitation curve:

$$V_{DC} = 2\pi f \cdot h^{-1}(I_{DC}) \tag{14}$$

For example, for the 10 percent GIC level in our sample CT, we obtain $h^{-1}(0.5 \text{ A}) = 0.0531$ Vs (meaning 0.5 A dc corresponds to the flux linkage of 0.0531 Vs, as in Fig. 20), and therefore, $V_{DC} = 20$ V.

The extra 20 V (peak) corresponds to the voltage drop across the burden resistance caused by an effective rms current calculated as follows:

$$I_{AC0} = \frac{V_{DC}}{\sqrt{2} \cdot R_B} \tag{15}$$

Following our numerical example, we obtain $I_{AC0} = 20$ V / ($\sqrt{2}$ • 0.1941 Ω) = 73 A rms secondary, or 14.6 pu. In other words, when considering transient saturation, the 0.1 pu dc is equivalent to the ac current of 14.6 pu rms.

This example shows that the impact is significant; to remove the effect of the dc component of only 10 percent of CT rated, we need to reduce the ac component by 14.6 times CT rated. To finalize our example, we check to see if reducing the ac current from 20 pu to 5.4 pu for the case of Fig. 29

gives us a similar result as for the case of 20 pu fault current with no standing dc current (Fig. 28).

Fig. 35 plots the relevant signals. Comparing Fig. 28 (20 pu fault current, no GIC) and Fig. 35 (fault current derated to 5.4 pu to account for the GIC of 0.1 pu) and focusing on the first cycle, we see that the transient CT response is very similar in both cases.
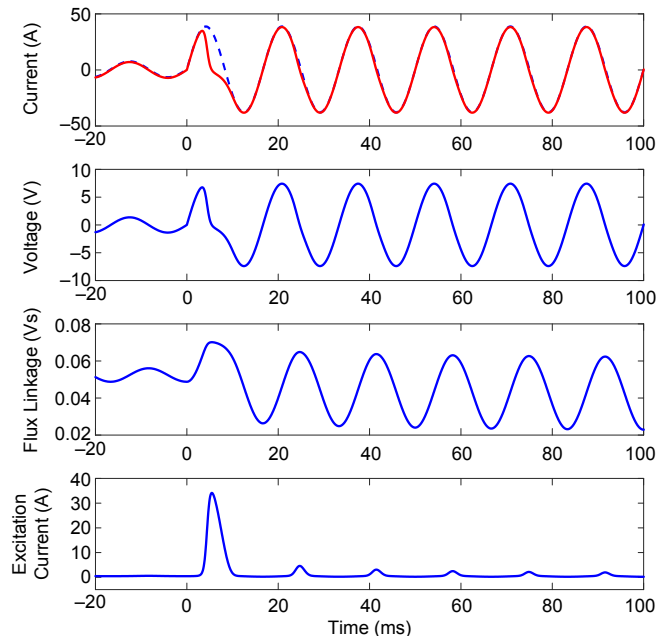

Fig. 35.   Response of the sample CT to the fault with the GIC component of 10 percent of rated. The fault current is 5.4 pu, following the derating rule proposed in this paper (computer simulation): primary ratio current (blue dashed), secondary current (red), secondary voltage, flux linkage, and excitation current.

To summarize this section, we can state the following:

- The small dc current representative of GIC has practically no impact on steady-state CT errors.
- A large dc component (well beyond GIC levels) would have a dramatic impact on the steady-state CT errors, but GIC cannot attain these large values when CTs are rated for transmission levels.
- Even the very small dc currents representative of GIC have a significant impact on transient saturation. Our example showed that a GIC of 10 percent of CT rated is equivalent to more than 10 times the CT rated ac current when it comes to transient CT errors.

VIII. IMPACT OF CT SATURATION CAUSED BY GICs ON PROTECTION

In the previous sections, we explained that steady-state CT errors due to practical GIC levels are minor. Protective relays are not designed or applied assuming perfect CT performance. We apply margins to cope with CT ratio errors and CT saturation.

We conclude the following with respect to protection elements that can be impacted by steady-state CT saturation due to GICs:

- Line distance and overcurrent elements may slightly underreach due to CT errors caused by GICs. This is not a concern for instantaneous tripping as these elements do underreach under normal conditions, such as due to fault resistance, and are therefore backed up by other protection elements. Time-coordinated distance or overcurrent elements apply margins, and with customary margins, they retain dependability, despite the GIC-caused CT errors.
- Line differential elements typically incorporate a means to address CT saturation, such as percentage restraint or the Alpha Plane [7], and they comfortably tolerate CT errors caused by the GICs in steady states.
- Transformer differential elements include percentage restraint to cope with CT errors, and they too remain secure for external faults even under GICs.

Transient CT saturation due to preexisting GICs can be very substantial. The saturation is, however, short-lived. We offer the following comments with respect to this:

- Distance and overcurrent relays would tend to underreach due to substantial CT saturation in the first half cycle of the fault current. As a result, we may see slightly delayed protection operation for in-zone faults due to transient CT saturation caused by the preexisting GICs. Again, the instantaneous distance and overcurrent elements are not 100 percent dependable (i.e., may not operate for resistive faults) and their slightly delayed operation will therefore not cause major problems and is not typically even noticed.
- Fast line differential relays may be affected by transient CT saturation, but these relays already guard against CT saturation, and when designed properly, do not face any problems. Slower line differential relays are secure because the errors during transient CT saturation from the GICs are short-lived.
- Similar points can be made about transformer differential relays.

We conclude that the impact of GIC-induced CT saturation on protective relays is minor. Slightly degraded dependability (underreaching, slower operation) is no different than for a number of other well-known factors. Existing means to deal with CT saturation due to the well-recognized factors ensure security for CT errors due to GICs. This observation can be better understood by noticing that the impact of GICs is similar to the impact of the CT remanent flux, and we do not see reports on many relay misoperations due to remanent flux in protection CTs.

Our takeaways are congruent with common observations and the lack of correlation between days of high geomagnetic activity and relay misoperations. We have studied data on unexpected relay operations and tried to correlate the data with the magnetic storm activity. We found no correlation at all.

IX. CONCLUSIONS

This paper provided a methodology to analyze the impact of GICs on protection CTs and derived a number of observations related to the topic.

The signal model of a CT, presented in Section III, is a very useful way of depicting the operation of a CT. The model aids understanding of all traditional aspects of CT fault performance, as well as the impact of GICs. This simplified model follows the well-known first principles, but its format, especially the excitation current acting as a nonlinear feedback control loop, aids better understanding of the CT operation for a number of conditions and factors.

Practical GIC levels have a minor impact on transmission-rated CTs in steady states. While completely saturated for the dc or low-frequency current, a CT reproduces the rated frequency current quite well. Protective relays are designed for this level of CT error, and therefore, perform well under the presence of GIC.

Even small GIC levels lead to transient CT saturation during faults. This phenomenon is very similar to the impact of remanent flux because fast and deep saturation can occur for the fault current, but the CT pulls out of this GIC-induced saturation very quickly (in a half cycle). While this effect is significant, it does not bring any new threats to the protection system. Slow relays, such as those using full-cycle filtering, are not affected. Fast relays, such as those operating in a half cycle or faster, already have the means to ensure security under fast and deep CT saturation.

The paper provided a methodology to derate a CT for the expected level of the GIC. When applied to guarantee saturation-free CT operation, this rule leads to a considerably oversized CT. This is similar to situations where we want to factor in a high remanent flux. We do not recommend applying such derating. Without this derating, the CT may saturate, but it pulls out of saturation very quickly. One may consider calculating the time to saturation while factoring in the GIC in order to ensure that fast differential relays have enough saturation-free data to engage their external fault detectors and ensure security.

Our analysis and findings explain why GIC-induced CT saturation is not a problem for present-day relays and why we do not see a correlation between high geomagnetic activity and unexpected relay operations.

X. REFERENCES

[1] S. E. Zocholl, *Analyzing and Applying Current Transformers*. Schweitzer Engineering Laboratories, Inc., Pullman, WA, 2004.

[2] H. J. Altuve, N. Fischer, G. Benmouyal, and D. Finney, "Sizing Current Transformers for Line Protection Applications," proceedings of the 66th Annual Conference for Protective Relay Engineers, College Station, TX, April 2013.

[3] J. G. Kappenman, V. D. Albertson, and N. Mohan, "Current Transformer and Relay Performance in the Presence of Geomagnetically-Induced Currents," *IEEE Transactions on Power Apparatus and Systems*, Vol. PAS-100, Issue 3, March 1981, pp.1078–1088.

[4] J. Elovaara, P. Lindblad, A. Viljanen, T. Mäkinen, R. Pirjola, S. Larsson, and B. Kielén, "Geomagnetically Induced Currents in the Nordic Power System and Their Effects on Equipment, Control, Protection and Operation," paper 36-301 of the proceedings of the CIGRE 1992 Session, Paris, France, 1992.

[5] National Oceanic and Atmospheric Administration, Space Weather Prediction Center, "Planetary K-Index," August 2015. Available: http://www.swpc.noaa.gov/products/planetary-k-index.

[6] R. Pirjola, "Geomagnetically Induced Currents During Magnetic Storms," *IEEE Transactions on Plasma Science*, Vol. 28, Issue 6, December 2000, pp.1867–1873.

[7] B. Kasztenny, G. Benmouyal, H. J. Altuve, and N. Fischer, "Tutorial on Operating Characteristics of Microprocessor-Based Multiterminal Line Current Differential Relays," proceedings of the 66th Annual Georgia Tech Protective Relaying Conference, Atlanta, GA, April 2012.

XI. Biographies

Bogdan Kasztenny is the R&D director of protection technology at Schweitzer Engineering Laboratories, Inc. He has over 25 years of expertise in power system protection and control, including 10 years of academic experience and 15 years of industrial experience, developing, promoting, and supporting many protection and control products. Bogdan is an IEEE Fellow, Senior Fulbright Fellow, Canadian representative of CIGRE Study Committee B5, registered professional engineer in the province of Ontario, and an adjunct professor at the University of Western Ontario. Since 2011, Bogdan has served on the Western Protective Relay Conference Program Committee. Bogdan has authored about 200 technical papers and holds 30 patents.

Norman Fischer received a Higher Diploma in Technology, with honors, from Technikon Witwatersrand, Johannesburg, South Africa, in 1988; a B.S.E.E., with honors, from the University of Cape Town in 1993; an M.S.E.E. from the University of Idaho in 2005; and a Ph.D. from the University of Idaho in 2014. He joined Eskom as a protection technician in 1984 and was a senior design engineer in the Eskom protection design department for three years. He then joined IST Energy as a senior design engineer in 1996. In 1999, Normann joined Schweitzer Engineering Laboratories, Inc., where he is currently a fellow engineer in the research and development division. He was a registered professional engineer in South Africa and a member of the South African Institute of Electrical Engineers. He is currently a senior member of IEEE and a member of the American Society for Engineering Education (ASEE).

Douglas Taylor received his B.S.E.E. and M.S.E.E. degrees from the University of Idaho in 2007 and 2009, respectively. Since 2009, he has worked at Schweitzer Engineering Laboratories, Inc. and currently is a lead research engineer in research and development. Mr. Taylor is a registered professional engineer in the state of Washington and is a member of the IEEE. His main interests are power system protection and power system analysis. He has authored several technical papers and holds one patent.

Tejasvi Prakash received his B.E. degree in electronics and communication from Bangalore University, India and his M.S.E.E. degree from the University of Idaho in 2000 and 2011, respectively. Mr. Prakash has extensive experience in condensed matter physics, nanomaterials synthesis, and device fabrication prior to joining Schweitzer Engineering Laboratories, Inc. in 2012. He is currently a research engineer in research and development, where he has focused on magnetic materials characterization in addition to new product development. He has several publications and holds one patent.

Jeevan Jalli received his B.Tech degree in metallurgical engineering from Visvesvaraya National Institute of Technology, Nagpur, India, in 2000; a M.S. degree in material science and engineering from the University of Idaho in 2007; and a Ph.D. in electrical engineering from The University of Alabama in 2014. In 2011, he joined Schweitzer Engineering Laboratories, Inc. and is currently a lead materials engineer in research and development. His research interests include soft magnetic materials for power applications, ferrites for RF devices, rare-earth free permanent magnets, and magnetic nanoparticles for high-density recording media. He has published and authored several technical papers and is a member of the IEEE and the American Ceramic Society.